Nanoribbon edges of transition-metal dichalcogenides: Stability and electronic properties

Daphne Davelou,[1,2,*] Georgios Kopidakis,[1,2] Efthimios Kaxiras,[3] and Ioannis N. Remediakis[1,2]
[1]*Department of Materials Science and Technology, University of Crete, Crete GR-70013, Heraklion, Greece*
[2]*Institute of Electronic Structure and Laser, Foundation for Research and Technology - Hellas, P.O. Box 1527, 71110 Heraklion, Crete, Greece*
[3]*Department of Physics and Harvard's Paulson School of Engineering and Applied Sciences, Harvard University, Cambridge, Massachusetts 02138, USA*

(Received 26 June 2017; revised manuscript received 8 October 2017; published 27 October 2017)

Nanoribbons of molybdenum disulfide (MoS_2) are interesting one-dimensional (1D) nanostructures with intriguing electronic properties, consisting of a semiconducting bulk bounded by edges with metallic character. Edges of similar character can also be expected in other transition-metal dichalcogenide (TMDC) nanostructures. We report first-principles electronic structure calculations for the total energy and the band structure of four representative TMDCs, MoS_2, $MoSe_2$, WS_2, WSe_2, in various 1D nanoribbon configurations. We compare the thermodynamic stability and the electronic structure of the 2D bulk and 35 different quasi-1D nanoribbons for each of the four materials. In each case, we consider the reconstructions of the zigzag metal-terminated edge by adding different amounts of chalcogen adatoms. The 1D structures we investigated have positive edge energies when the chalcogen chemical potential is close to the energy of the bulk chalcogen phase, and negative edge energies for higher chemical potential values. We find that the reconstruction with two chalcogen adatoms per edge metal atom is the most stable under usual experimental conditions and that all 1D nanoribbon structures exhibit metallic character.

DOI: 10.1103/PhysRevB.96.165436

I. INTRODUCTION

Layered materials are currently under intense investigation for their unique mechanical, electronic, and chemical properties. Of particular interest are transition-metal dichalcogenides (TMDCs) of the type MX_2, where M is a metal and X is a chalcogen [1]. Representative materials in this family are MoS_2, $MoSe_2$, WS_2, and WSe_2, which are semiconductors in both their three-dimensional (3D) and 2D structure [2–11], while new members are being constantly added [12]. There is strong evidence that MoS_2 is metallic in its quasi-1D structures [13–15].

Apart from being a model system for the structure of edges, MoS_2 nanoribbons have been studied extensively as they offer a unique electronic structure that combines features of MoS_2 and graphene. Bollinger *et al.* [14,15] predicted the existence of metallic edge states in MoS_2 nanoribbons using electronic structure calculations. Ridolfi *et al.* [16] studied the effect of short- and long-range disorder on MoS_2 zigzag nanoribbons, and found that the metallic states are robust against structural disorder. TMDC nanoribbons were later synthesized by Camacho-Bragado *et al.* attached to MoO_3 clusters [17] and by Wang *et al.* inside carbon nanotubes [18]. In that paper Wang *et al.* included DFT calculations that showed spin polarization at E_F for MoS_2 nanoribbons with a fully saturated Mo edge by S atoms. This level of treatment far exceeds what is feasible to handle for the nanoribbons considered here. Theoretical studies also include the work of Li *et al.* [19] who performed spin-polarized calculations and predicted that zigzag MoS_2 nanoribbons are magnetic and are more stable than triangular nanoclusters, Kou *et al.* [20] who showed that strain and applied electric field can alter dramatically both magnetic and electronic behavior, and Kim *et al.* [21] who found that armchair nanoribbons can be stabilized by H adsorption and possess a semiconducting character with strong excitonic effects. Presence of metallic edges seems to be a general feature of hexagonal 2D materials [22,23]. In previous work [24], we reported that the metallic edges alter the dielectric permitivity of the nanoribbons and that the spatial extent of this effect is around 5 Å from the edge of the material. Finally, MoS_2 nanoribbons could play a key role in the hydrogen evolution reaction [25,26], and graphene support enhances these features [27,28]. Yu *et al.* [29] verified the tunability of edge states through the use of external electric fields and hydrogen absorption.

Although the stability of metallic states in MoS_2 and their electronic structure is well established [15,30], little is known about nanoribbons of $MoSe_2$, WS_2, and WSe_2. Here, we address two issues related to the properties of nanoribbons of these materials: First, we examine the thermodynamic stability of various types nanoribbon edges under relevant experimental conditions. The limited number of synthesis reports implies that such structures might be unfavorable, while their use in catalysis confirms that, once formed, these structures are extremely stable. Second, we examine how robust the edge-related metallic states are and what is the position of the Fermi level of the metallic region relative to the Fermi level of the 2D bulk.

II. COMPUTATIONAL METHODOLOGY

To construct the nanoribbons, we start from a rectangular repeat unit (see Fig. 1) with sides of length a along the $\hat{x}$ and $a\sqrt{3}$ along the $\hat{y}$ directions, where a is the lattice constant of the 2D material [10]. In relation to the original lattice vectors $\mathbf{a}_1, \mathbf{a}_2$ of the honeycomb lattice, which is the underlying crystal lattice for the bulk 2D layer of the TMDCs, the new vectors

*d.davelou@materials.uoc.gr

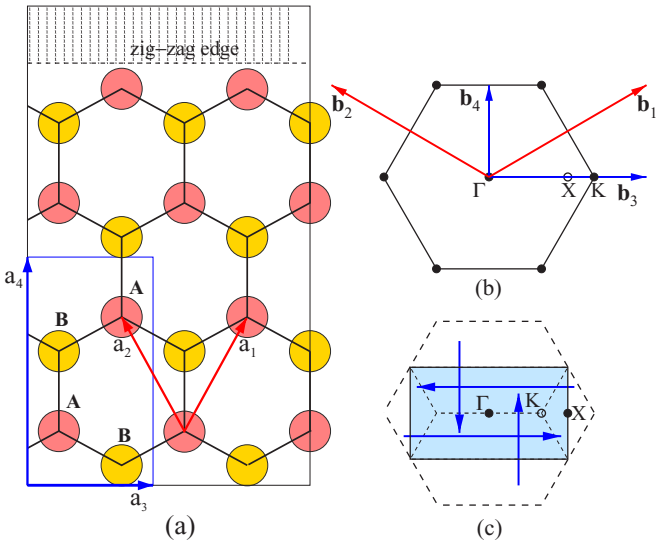

FIG. 1. (a) Definition of the repeat unit (blue rectangle) and the repeat vectors $\mathbf{a}_3$, (x direction) $\mathbf{a}_4$ (y direction) (blue arrows) and original lattice vectors $\mathbf{a}_1$, $\mathbf{a}_2$ (red arrows). (b) Brillouin zone of the bulk 2D structure, with the original reciprocal lattice vectors $\mathbf{b}_1$, $\mathbf{b}_2$ (red arrows) and the new vectors $\mathbf{b}_3$, $\mathbf{b}_4$ (blue arrows) corresponding to the rectangular repeat unit. (c) Folding of the original BZ (dashed black lines) to the new BZ (solid black lines) through the mapping by displacements of $\pm\mathbf{b}_3$, $\pm\mathbf{b}_4$. The positions of special $\mathbf{k}$ points Γ, K, and X are marked by solid and open dots.

that describe the repeat unit are given by: $\mathbf{a}_3 = \mathbf{a}_1 - \mathbf{a}_2, \mathbf{a}_4 = \mathbf{a}_1 + \mathbf{a}_2$. This repeat unit contains two metal (M) and four chalcogen (X) atoms, at the sites labeled A and B in Fig. 1. In this figure, red circles (marked A) represent the positions of M atoms and yellow circles (marked B) represent the projections of X atoms on the plane. We construct a supercell by repeating this unit cell n_c times along the $\hat{y}$ direction, and then a vacuum region is added along the $\hat{y}$ and $\hat{z}$ directions. Periodic boundary conditions are imposed along all directions. In the y and z directions, adjacent slabs are separated by 12.0 Å of vacuum. For few test systems, we repeated the calculation with open boundary conditions along these directions, where the wave functions and density vanish at the edges of the simulation box. The two methods give identical results. The structure formed is a nanoribbon of infinite length along $\hat{x}$ and has a width of n_c cells along $\hat{y}$, with $1 \leqslant n_c \leqslant 7$. This corresponds to nanoribbon widths in the range of 5.5 Å to 42 Å. The Brillouin zone (BZ) that corresponds to the new crystal structure defined by the repeat unit is a subspace of the original BZ of the honeycomb lattice, due to folding by the new reciprocal vectors $\mathbf{b}_3$, $\mathbf{b}_4$, as shown explicitly in Fig. 1(c). This results in the edge point K of the original BZ being mapped onto an interior point in the new BZ, while the interior point X of the original BZ becomes an edge point in the new BZ. These features are important in interpreting the band structures of the nanoribbons discussed in the following section.

We perform first-principles electronic structure and total-energy calculations based on Density Functional Theory (DFT), using the real-space Grid-Based Projector Augmented-Wave [31] (GPAW) package [32,33]. For the exchange-correlation functional we use the Generalized Gradient Approximation (GGA) of Perdew-Burke-Ernzerhof (PBE) [34]. Although the PBE functional is not the preferred choice for the calculation of the band structure due to its underestimation of the energy gap [35], the use of hybrid functionals and/or many-body equations to treat accurately the excitonic effects [36–38] is beyond the scope of the present work, as we focus on ground-state properties or trends for the electronic features. In GPAW, the computational parameters that need to be taken into account are the grid spacing, h, the number of Monkhorst-Pack $\mathbf{k}$ points for sampling of the Brillouin zone and the thickness of the vacuum region, L_V, beyond the last atoms of the system. The parameters used in our study are $h \approx 0.19$ Å, $4 \times 1 \times 1$ $\mathbf{k}$ points and $L_V = 12.0$ Å.

For every width, n_c, we consider five different terminations of the M edge. These terminations correspond to N_X ($0 \leqslant N_X \leqslant 4$) X adatoms decorating the M edge. The geometrical configuration for the case with two chalcogen adatoms was chosen to be that of a dimer that lies perpendicular to the layer, in accordance with several theoretical (Bollinger *et al.* [14], Byskov *et al.* [39]) and experimental (Helveg *et al.* [13]) observations. All the other structures with two adatoms we tried yield much higher edge energies, by 0.23 eV/Å or more, above the edge energy of the structure with the dimer. For structures with three and four adatoms, we tried several different structures in order to identify the one with lowest energy; in all cases, the structures with twofold S atoms have the lowest edge energy. We used the atomic simulation environment (ASE) suite [40] for the generation of structures, atomic relaxation, and analysis of the results. For the X edge we do not expect any reconstruction other than changes in bond lengths [41]. In total, we consider 35 nanoribbon structures for each material and we took into account the full relaxation of atom positions in the first two atomic rows from both edges, as well as all adatom positions. The relaxed structures of five typical MX_2 nanoribbons for $n_c = 2$ are shown in Fig. 2. In all cases, chalcogen adatoms are twofold coordinated and have similar bond lengths as in the bulk of the material.

III. RESULTS AND DISCUSSION

A. Thermodynamic stability

The key quantity that determines the stability of nanoribbons, relative to the bulk 2D layer, is the edge energy, γ. This is the one-dimensional analog of surface energy (surface tension), that is, the energy per unit length needed to cleave the material. A 2D material in vacuum is expected to have $\gamma > 0$, as it costs energy to break chemical bonds and create an edge. For a 2D material in equilibrium with an active compound, the edge energy will be different, as new bonds can be formed between edge atoms and atoms of molecules coming from the reservoir. By applying a general formula for the solid-gas interfacial tension [42,43], we can write

$$\gamma = \gamma_0 - E/L, \tag{1}$$

where γ_0 is the edge energy in vacuum, E is the average energy of any new bonds that are formed and L is the average distance between such new bonds. From Eq. (1) it is clear that γ could be either negative or positive, depending on the strength and density of the bonds between edge atoms and atoms/molecules of the reservoir. A negative value of γ means that the ripping of

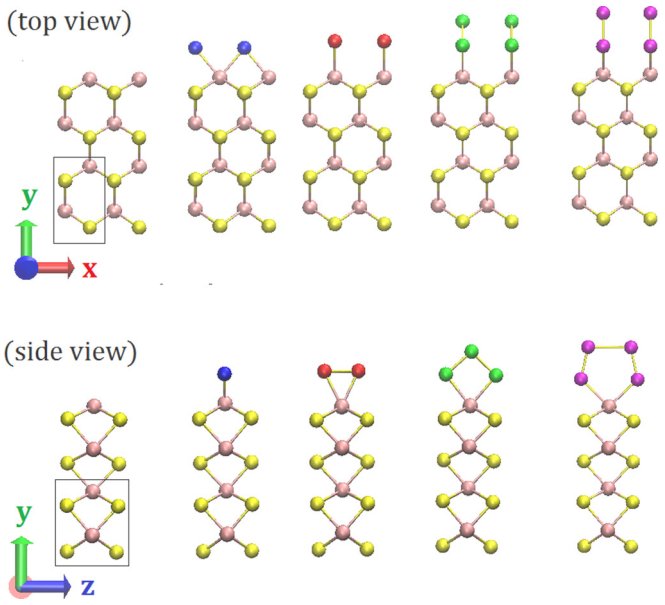

FIG. 2. Structural models (top and side views) of relaxed structures of typical nanoribbons (MX_2 with $n_c = 2$) with increasing number of adatoms N_X, from zero (left) to four (right), at the metal-terminated zigzag edge. Two unit cells along the x direction of the periodic structure, are shown. Pink and yellow spheres represent the metal and chalcogen atoms, respectively. The extra chalcogen adatoms are color coded blue ($N_X = 1$), red ($N_X = 2$), green ($N_X = 3$), and purple ($N_X = 4$), for reference in the following figures.

the material and formation of edges is an exothermic process, whereas ripping of the material is endothermic for $\gamma > 0$.

The edge energy, γ, is defined in a similar way as the surface energy of 3D materials: A nanoribbon made of MX_2 has total energy

$$E_{\text{tot}} = 2n_c E_{MX_2} + N_X \mu_X + 2a\gamma, \tag{2}$$

where E_{MX_2} is the energy of the monolayer per MX_2 unit, $2n_c$ is the number of MX_2 units along the $\hat{y}$ direction, N_X is the number of chalcogen adatoms at the reconstructed edge and μ_X is the chemical potential of the chalcogen X. The last term is the energy cost associated with the formation of the two edges, which is proportional to the length of the unit cell along $\hat{x}$, a, and the edge energy, γ. The edge energy is calculated by plotting E_{tot} as a function of n_c and then using a least-squares method to fit a straight line to the calculations [24].

The chemical potential μ_X of chalcogen X (S or Se) is an important parameter that links the theoretical modeling to experimental conditions. In principle, the nanoribbons are in equilibrium with a reservoir of X atoms, and μ_X is the energy required to take one X atom from this reservoir. No matter what the X-containing compound is, μ_X cannot be greater than the energy of an isolated X atom (where the atom has no chemical bonds), and it cannot be lower than the energy of the solid bulk form of X, which is the preferred state of X at standard conditions. In order to establish reliable values for the chalcogen chemical potentials, we investigate the cohesive energy of their bulk structures. Chalcogens have some of the most complicated crystal structures for elemental solids [44]. A full DFT study of these structures is a demanding project in itself, beyond the scope of the present work. We limited ourselves to calculations of metastable structures that are simpler than the standard bulk forms of the chalcogen materials, while maintaining the same local environment around each chalcogen atom as in the bulk. Both chalcogens prefer to form structures with twofold coordination, where rings of atoms are arranged periodically in space. The rhombohedral structure of S is modeled using a hexagonal unit cell that contains three rings of six S atoms. The structure of α-monoclinic Se has a unit cell that contains four eight-membered rings. We consider the cohesive energy of S and Se in these model structures, which is the difference in energy between an isolated atom and an atom in the solid. We compare these values to the atomization energies of these materials [45]. The calculations are in excellent agreement to experimental data: the cohesive energy of S is found to be 2.82 eV (experimental value is 2.87 eV) while that of Se is found to be 2.43 eV (experimental value is 2.35 eV). This comparison establishes that our assumptions for the chalcogen chemical potentials are very reasonable.

The results for the dependence of the edge energy on the chemical potential of chalcogens are shown in Fig. 3. For purposes of comparison between the four materials we present the same range for the chalcogen chemical potential, starting at the bulk value. We give the chalcogen chemical potential with reference to the the value of a chalcogen atom at zero pressure and temperature, and we indicate the values corresponding to the respective bulk elemental solids. The experimentally relevant region is the range of values larger than those limiting values. In chemical compounds of chalcogens (such as alkanethiols), X forms the same number of covalent bonds as in solid X, and should have similar energy (although somewhat higher than in its standard form).

Depending on the value of the edge energy, we expect that when a single layer of a TMDC material is exposed to a chalcogen environment, it will either remain intact ($\gamma > 0$) or, when $\gamma < 0$, the structure will be unstable. For all four materials, we find that $\gamma < 0$ when $\mu_X \sim 0$, the limit at which X atoms can lower their energy by leaving the gas phase and become incorporated into the TMDC edge. For this reason, the structure with the largest possible number of chalcogen atoms (in our study $N_X = 4$) is always favored for high values of μ_X. Moreover, γ is negative in all cases when the chemical potential is about 0.5 eV above the energy of the solid. This means that edges will be formed spontaneously if the 2D material is at equilibrium with compounds where the chalcogen atoms are weakly bound. On the other hand, $\gamma > 0$ for chalcogen chemical potential near that of the solid phase, which means that TMDC layers will be stable with respect to most sulfides and selenides, and are vulnerable to ripping only when in contact with atomic chalcogens or radicals.

The plots of Fig. 3 also reveal the favorable number of adatoms for each material, that is, the number N_X that corresponds to the lowest-energy structure. The metal-terminated edge has energy that is significantly higher (by about 0.3 eV/Å) than the energy of any other edge, implying that stable 1D nanoribbon structures will be formed by attracting chalcogen atoms at the zigzag edge, once they are exposed to an external source. In the case of solid S or Se reservoirs,

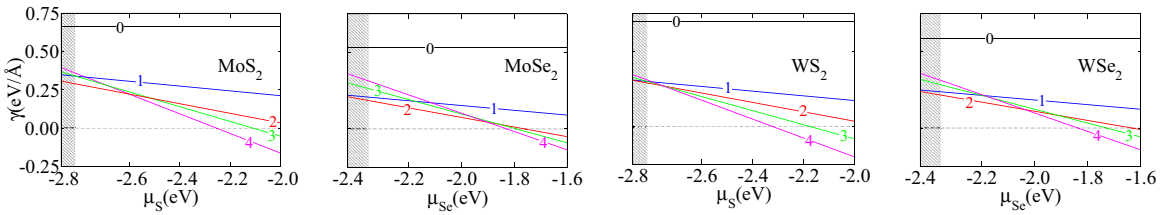

FIG. 3. Edge energies, γ, of MX_2 nanoribbons with different number of adatoms, as a function of the chalcogen chemical potential, μ_X relative to the chemical potential of atomic X (M = Mo, W; X = S, Se). Different colors correspond to different number of adatoms, as in Fig. 2. The shaded vertical column indicates the range of values of the bulk chalcogen chemical potential. For S adatoms, the lower value is the experimental result, the upper value the theoretical result, while the opposite is the case for Se.

the preferred number of adatoms at the reconstructed edge is $N_X = 2$ for all four materials. For MoS_2 in particular, our findings are in excellent agreement to experiments that found complete absence of M-terminated edges and preference for edges terminated by S dimers [17]. For higher values of the chemical potential, the preferred amount of adatoms at the edge increases, as expected. In the case of atomic source, the edge energies of the nanoribbons is lowered by 0.3 eV/Å to 0.4 eV/Å per extra adatom. Only the structures with $N_X = 2$ or 4 are stable, since other terminations of the nanoribbons have higher energy at any value of the chemical potentials.

We conclude from this analysis that stable nanoribbon edges will have termination consisting of two chalcogen adatoms for chemical potential values close to the bulk chalcogen phases, or four chalcogen adatoms for chemical potential values higher than the bulk phase (by 0.1–0.2 eV for S compounds and by 0.3–0.5 eV for Se compounds); under no plausible conditions the edges will have metal-atom termination.

B. Electronic properties

Dimensionality plays a key role in the electronic structure of TMDCs. In 3D structures, all materials considered here are indirect gap semiconductors [46], while in each case the 2D single-layer structure is a direct gap semiconductor [10,47]. This shift of the energy gap from K-Γ to K-K points of the Brillouin zone is responsible for the observed photoluminescence.

The density of states (DOS) of a TMDC nanoribbon includes a characteristic peak at the Fermi level, E_F, surrounded by a few lower peaks that also lie inside the gap of the 2D material. These states are localized at the upper and lower edge of the nanoribbon along the $\hat{y}$ direction and resemble electrons confined in one dimension. We observe the same behavior in all TMDCs, all widths and all numbers of chalcogen adatoms: there is a clear peak at E_F, the height of which decreases for increasing nanoribbon width, n_c. At $n_c \to \infty$, the peak is expected to disappear. The reason for this width dependence is the following: In the valence band of a nanoribbon with width n_c and N_X adatoms there are $18n_c + 3N_X$ occupied electronic states for each **k** point in the Brillouin zone, only few of which are edge states. The contribution of edge states becomes negligible for large n_c.

In Fig. 4 we present the DOS of nanoribbons with width $n_c = 6$. At this width, there are enough bulk states to represent the DOS of the 2D material, while the edge states are still prominent and have impact on the properties of the system. The DOS alone might not be enough to characterize the edge states as metallic, as it is important to verify that indeed the Fermi level of the nanoribbon lies within the gap of the 2D material. Aligning the DOS of two systems with different numbers of atoms in order to calculate the difference of their Fermi levels is a nontrivial task. Here, we adopt a simple procedure, which is based on the assumption that states at the lowest edge of the valence band are not affected by the presence of the edge in the material.

Our DOS calculations support this idea, as all of them possess identical peaks at low energies (in the range of −10 eV, not shown in Fig. 4), regardless of edge structure and nanoribbon width. We shift the energy of electronic states of nanoribbons until those low-energy peaks are aligned with the corresponding peaks from the DOS of the 2D bulk. To make the comparison as accurate as possible, we recalculate the DOS of the 2D bulk using an identical unit cell with the same number of atoms and dimensions as in the case of

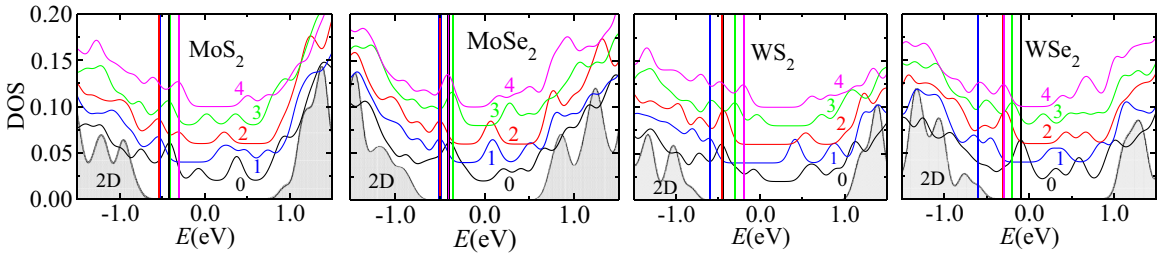

FIG. 4. Density of states for bulk 2D MX_2 (gray filled area) and the MX_2 nanoribbons (colored solid lines, with the same scheme as in Fig. 2). The energy range is within 1.5 eV of the midgap point, which is set to zero, the Fermi levels of the nanoribbons are shown with color-coded vertical lines. The curves for the DOS of the nanoribbons with N_X adatoms have been shifted vertically by $0.2(N_X + 1)$ eV for clarity.

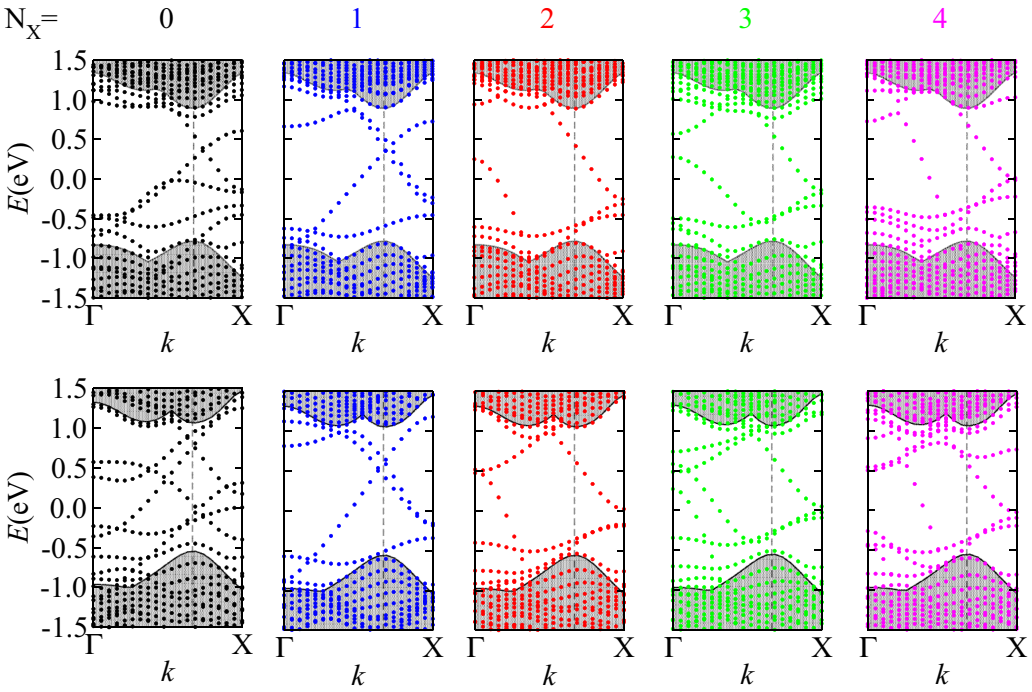

FIG. 5. Band structures of the MoS_2 (top row) and WSe_2 (bottom row) nanoribbons of width $n_c = 6$ and different number N_X of chalcogen adatoms along the zigzag edge. The gray filled area shows the band structure of the 2D bulk in each case. The zero of the energy scale is set to the Fermi level of the ideal single layer. The dashed vertical line indicates the K point of the BZ.

nanoribbons with width $n_c = 6$ and metal-terminated edge. At low energies, sulfides have three characteristic peaks, a doublet and a singlet, while selenides have a triplet and a singlet peak. We chose the shift of energies so that the average error from these peaks is minimized. With this alignment, we find that the position of the Fermi level of the nanoribbons is always lower in energy compared to that of the single-layer bulk. All nanoribbons have Fermi levels that lie inside the gap of the 2D bulk, which establishes the metallic character of the zigzag edges of TMDC nanoribbons, due to the edge states. In the most stable structures, with $N_X = 2$ chalcogen adatoms and for a width of $n_c = 6$, the nanoribbon Fermi level is pinned at about -0.3 eV to -0.5 eV below that of the 2D bulk, for all materials.

Figure 5 shows the band structures for MoS_2 and WSe_2 nanoribbons of width $n_c = 6$. Similar behavior is observed in $MoSe_2$ and WS_2 as well. The energies are given relative to the Fermi level of the 2D bulk. In all plots, the projection of the underlying band structure of the 2D bulk is shown as a shaded area. For MoS_2, the valence band maximum of the 2D system is at about -0.75 eV while the conduction band mimimum is at about 0.85 eV, resulting at a band gap of 1.6 eV. The gap is direct, as the two extrema occur at the same **k** point, which lies at $2/3$ of the distance from Γ to X, the edge of the 1D Brillouin zone. The point where the direct gap occurs corresponds to the K point of the Brillouin zone for the 2D hexagonal structure, due to folding from the definition of the primitive vectors of the unit cell, as shown in Fig. 1. In all cases, the band gap of the 2D material is crossed by several bands, which are not flat, as one might have expected for localized defect states. These states correspond to metallic character, describing electrons that move in one-dimensional Bloch states along the edge.

IV. CONCLUSIONS

We performed a systematic set of first-principles calculations for TMDC nanoribbons of four different materials (MoS_2, $MoSe_2$, WS_2, and WSe_2), of width between 5.5 Å and 42 Å, with edge structure containing various amounts of chalcogen X atoms, $0 \leqslant N_X \leqslant 4$, attached to the metal-terminated edge. We examined the thermodynamic stability of these nanoribbons at equilibrium with different chalcogen reservoirs. We find that nanoribbons with $N_X = 2$ adatoms are most stable with respect to the bulk chalcogen phase or stable molecules such as thiols, while $N_X = 4$ is favored when weakly bound chalcogen compounds are available.

While the 2D materials are semiconductors, TMDC nanoribbons with zigzag edges are always metallic regardless of the composition, the width, or the edge structure. The Fermi level of the metallic phase is always lower in energy than the Fermi level of the 2D bulk, thus making it favorable for electrons to occupy these metallic states. The bands of the edge states are one-dimensional Bloch states with large dispersion, extending across the band gap of the 2D layer. The presence of edge metallic states in a 2D bulk semiconductor, common to all the cases considered here, with bands crossing the gap and states that are stable against chemical modification of the edges, led to the suggestion [24] that TMDC nanoribbons could be candidates for topological insulator behavior.

ACKNOWLEDGMENTS

The authors thank Dr. Wei Chen for a critical reading of the manuscript. This work was supported by the Research Committee of the University of Crete (K.A. 4046 and 4180),

by the Greek GSRT project ERC02-EXEL Grant No. 6260, by EC FET Graphene Flagship and by the Cy-Tera Project. E.K. acknowledges support from ARO MURI Award No. W911NF-14-0247, and thanks the Crete Center of Quantum Complexity and Nanotechnology for its hospitality, through Marie-Curie RISE project NHQWAVE No. 691209.

[1] Q. H. Wang, K. Kalantar-Zadeh, A. Kis, J. N. Coleman, and M. S. Strano, Nature Nanotechnol. **7**, 699 (2012).
[2] K. F. Mak, C. Lee, J. Hone, J. Shan, and T. F. Heinz, Phys. Rev. Lett. **105**, 136805 (2010).
[3] A. Splendiani, L. Sun, Y. Zhang, T. Li, J. Kim, C.-Y. Chim, G. Galli, and F. Wang, Nano Lett. **10**, 1271 (2010).
[4] A. Kuc, N. Zibouche, and T. Heine, Phys. Rev. B **83**, 245213 (2011).
[5] Y. Ding, Y. Wang, J. Ni, L. Shi, S. Shi, and W. Tang, Physica B (Amsterdam) **406**, 2254 (2011).
[6] L. Liu, S. B. Kumar, Y. Ouyang, and J. Guo, IEEE Trans. Electron Devices **58**, 3042 (2011).
[7] E. S. Kadantsev and P. Hawrylak, Solid State Commun. **152**, 909 (2012).
[8] G. A. Tritsaris, B. D. Malone, and E. Kaxiras, J. Appl. Phys. **113**, 233507 (2013).
[9] E. J. G. Santos and E. Kaxiras, ACS Nano **7**, 10741 (2013).
[10] A. E. Maniadaki, G. Kopidakis, and I. N. Remediakis, Solid State Commun. **227**, 33 (2016).
[11] W. Chen, E. J. G. Santos, W. Zhu, E. Kaxiras, and Z. Zhang, Nano Lett. **13**, 509 (2013).
[12] S. Lebègue, T. Björkman, M. Klintenberg, R. M. Nieminen, and O. Eriksson, Phys. Rev. X **3**, 031002 (2013).
[13] S. Helveg, J. V. Lauritsen, E. Lægsgaard, I. Stensgaard, J. K. Nørskov, B. S. Clausen, H. Topsøe, and F. Besenbacher, Phys. Rev. Lett. **84**, 951 (2000).
[14] M. V. Bollinger, J. V. Lauritsen, K. W. Jacobsen, J. K. Nørskov, S. Helveg, and F. Besenbacher, Phys. Rev. Lett. **87**, 196803 (2001).
[15] M. V. Bollinger, K. W. Jacobsen, and J. K. Nørskov, Phys. Rev. B **67**, 085410 (2003).
[16] E. Ridolfi, L. R. F. Lima, E. R. Mucciolo, and C. H. Lewenkopf, Phys. Rev. B **95**, 035430 (2017).
[17] G. Camacho-Bragado, J. Elechiguerra, A. Olivas, S. Fuentes, D. Galvan, and M. J. Yacaman, J. Catal. **234**, 182 (2005).
[18] Z. Wang, H. Li, Z. Liu, Z. Shi, J. Lu, K. Suenaga, S.-K. Joung, T. Okazaki, Z. Gu, J. Zhou, Z. Gao, G. Li, S. Sanvito, E. Wang, and S. Iijima, J. Am. Chem. Soc. **132**, 13840 (2010).
[19] Y. Li, Z. Zhou, S. Zhang, and Z. Chen, J. Am. Chem. Soc. **130**, 16739 (2008).
[20] L. Kou, C. Tang, Y. Zhang, T. Heine, C. Chen, and T. Frauenheim, J. Phys. Chem. Lett. **3**, 2934 (2012).
[21] J. Kim, W. S. Yun, and J. D. Lee, J. Phys. Chem. C **119**, 13901 (2015).
[22] M. Gibertini, G. Pizzi, and N. Marzari, Nature Commun. **5**, 5157 (2014).
[23] M. Gibertini and N. Marzari, Nano Lett. **15**, 6229 (2015).
[24] D. Davelou, G. Kopidakis, G. Kioseoglou, and I. N. Remediakis, Solid State Commun. **192**, 42 (2014).
[25] B. Hinnemann, P. G. Moses, J. Bonde, K. P. Jørgensen, J. H. Nielsen, S. Horch, I. Chorkendorff, and J. K. Nørskov, J. Am. Chem. Soc. **127**, 5308 (2005).
[26] B. Hinnemann, J. K. Nørskov, and H. Topsøe, J. Phys. Chem. B **109**, 2245 (2005).
[27] A. E. Maniadaki and G. Kopidakis, Phys. Status Solidi Rapid Res. Lett. **10**, 453 (2016).
[28] C. Tsai, F. Abild-Pedersen, and J. K. Nørskov, Nano Lett. **14**, 1381 (2014).
[29] S. Yu and W. Zheng, Phys. Chem. Chem. Phys. **18**, 4675 (2016).
[30] D. Cao, T. Shen, P. Liang, X. Chen, and H. Shu, J. Phys. Chem. C **119**, 4294 (2015).
[31] P. E. Blöchl, Phys. Rev. B **50**, 17953 (1994).
[32] J. J. Mortensen, L. B. Hansen, and K. W. Jacobsen, Phys. Rev. B **71**, 035109 (2005).
[33] J. Enkovaara, C. Rostgaard, J. J. Mortensen, J. Chen, M. Dułak, L. Ferrighi, J. Gavnholt, C. Glinsvad, V. Haikola, H. A. Hansen, H. H. Kristoffersen, M. Kuisma, A. H. Larsen, L. Lehtovaara, M. Ljungberg, O. Lopez-Acevedo, P. G. Moses, J. Ojanen, T. Olsen, V. Petzold, N. A. Romero, J. Stausholm-Møller, M. Strange, G. A. Tritsaris, M. Vanin, M. Walter, B. Hammer, H. Häkkinen, G. K. H. Madsen, R. M. Nieminen, J. K. Nørskov, M. Puska, T. T. Rantala, J. Schiøtz, K. S. Thygesen, and K. W. Jacobsen, J. Phys.: Condens. Matter **22**, 253202 (2010).
[34] J. P. Perdew, K. Burke, and M. Ernzerhof, Phys. Rev. Lett. **77**, 3865 (1996).
[35] D. Y. Qiu, F. H. da Jornada, and S. G. Louie, Phys. Rev. Lett. **111**, 216805 (2013).
[36] A. Ramasubramaniam, Phys. Rev. B **86**, 115409 (2012).
[37] G. R. Bhimanapati, Z. Lin, V. Meunier, Y. Jung, J. Cha, S. Das, D. Xiao, Y. Son, M. S. Strano, V. R. Cooper, L. Liang, S. G. Louie, E. Ringe, W. Zhou, S. S. Kim, R. R. Naik, B. G. Sumpter, H. Terrones, F. Xia, Y. Wang, J. Zhu, D. Akinwande, N. Alem, J. A. Schuller, R. E. Schaak, M. Terrones, and J. A. Robinson, ACS Nano **9**, 11509 (2015).
[38] D. Y. Qiu, F. H. da Jornada, and S. G. Louie, Phys. Rev. B **93**, 235435 (2016).
[39] L. S. Byskov,J. K. Nørskov, B. S. Clausen, and H. Topsøe, Cat. Lett. **64**, 95 (2000).
[40] S. R. Bahn and K. W. Jacobsen, Comput. Sci. Eng. **4**, 56 (2002).
[41] P. Cui, J.-H. Choi, W. Chen, J. Zeng, C.-K. Shih, Z. Li, and Z. Zhang, Nano Lett. **17**, 1097 (2017).
[42] G. D. Barmparis and I. N. Remediakis, Phys. Rev. B **86**, 085457 (2012).
[43] G. D. Barmparis, Z. Lodziana, N. Lopez, and I. N. Remediakis, Beilstein J. Nanotechnol. **6**, 361 (2015).
[44] R. W. G. Wyckoff, *Crystal Structures*, 2nd ed. (Interscience Publishers, New York, 1963).
[45] Data from www.webelements.com (accessed Nov 17, 2016).
[46] K. K. Kam and B. A. Parkinson, J. Phys. Chem. **86**, 463 (1982).
[47] A. Kumar and P. K. Ahluwalia, Europhys. J. B **85**, 1 (2012).